

Strong Single- and Two-Photon Luminescence Enhancement by Non-Radiative Energy Transfer across Layered Heterostructure

Medha Dandu, Rabindra Biswas, Sarthak Das, Sangeeth Kallatt, Suman Chatterjee, Mehak Mahajan, Varun Raghunathan, Kausik Majumdar*

Department of Electrical Communication Engineering, Indian Institute of Science, Bangalore 560012, India.

*Corresponding author, email: kausikm@iisc.ac.in

ABSTRACT: The strong light-matter interaction in monolayer transition metal dichalcogenides (TMDs) is promising for nanoscale optoelectronics with their direct band gap nature and the ultra-fast radiative decay of the strongly bound excitons these materials host. However, the impeded amount of light absorption imposed by the ultra-thin nature of the monolayers impairs their viability in photonic applications. Using a layered heterostructure of a monolayer TMD stacked on top of strongly absorbing, non-luminescent, multi-layer SnSe₂, we show that both single-photon and two-photon luminescence from the TMD monolayer can be enhanced by a factor of 14 and 7.5, respectively. This is enabled through inter-layer dipole-dipole coupling induced non-radiative Förster resonance energy transfer (FRET) from SnSe₂ underneath which acts as a scavenger of the light unabsorbed by the monolayer TMD. The design strategy exploits the near-resonance between the direct energy gap of SnSe₂ and the excitonic gap of monolayer TMD, the smallest possible separation between donor and acceptor facilitated by van der Waals heterojunction, and the in-plane orientation of dipoles in these layered materials. The FRET driven uniform single- and two-photon luminescence enhancement over the entire junction area is advantageous over the local enhancement in quantum dot or plasmonic structure integrated 2D layers, and is promising for improving quantum efficiency in imaging, optoelectronic, and photonic applications.

KEYWORDS: MoS₂, WS₂, SnSe₂, van der Waals heterostructure, photoluminescence enhancement, two-photon luminescence, Förster Resonance Energy Transfer (FRET), charge transfer.

Monolayer transition metal dichalcogenides (TMDs) exhibit direct band gap with reduced dielectric screening and strong quantum confinement that enhance coulomb interactions to form strongly bound excitons under illumination.¹⁻⁴ Highly efficient luminescence due to a rapid radiative decay of excitons in TMDs⁵⁻⁸ instilled extensive interest for using these layered materials in the design of optoelectronic devices. Additionally, TMDs have also been explored for non-linear optical phenomena such as ultrafast saturable absorption, two-photon absorption and harmonic generation which are promising for photonic applications.⁹ However, the weak light absorption in a monolayer TMD¹⁰ due to its ultra-thin nature curtails its single and two-photon luminescence regardless of their inherent strength of the light-matter interactions.

Enhanced photoluminescence (PL) from monolayer TMDs has been demonstrated by coupling them with complementing optical platforms like mirco/nano-cavities,¹¹ photonic crystals¹² and hybrid reflectors.^{13,14} Recent integration of plasmonic structures with TMDs have reported very high enhancement factors of PL from TMD.^{15,16} This results from a combination of Purcell effect and local enhancement of electric field. Chemically driven surface modification for defect passivation and functionalization with quantum dots are also found to be effective in enhancing TMD PL.^{17,18} QDs assembled on monolayer TMDs show PL enhancement in the TMD and PL quenching in the QD coupled with a reduction in its exciton radiative lifetime proving the existence of Förster Resonance Energy Transfer (FRET).¹⁹ Such non-radiative energy transfer is enabled by dipole-dipole coupling between the donor and the acceptor and its rate is governed by their spectral overlap, physical separation, orientation of dipoles and corresponding oscillator strengths.²⁰

It would be interesting to exploit FRET across layered heterostructures where each layer has large excitonic oscillator strengths with a possibility of matching of in-plane center of mass momentum, facilitating dipolar coupling.²¹ Kozawa *et al.*²² showed the evidence for fast interlayer energy

transfer across WS₂/MoSe₂ hetero-bilayer stack through FRET across higher order exciton transitions. Nonetheless, the donor's absorption is still constrained by its physical thickness at the monolayer limit despite the high efficiency of FRET at the closest possible physical separation.

Here, we demonstrate enhanced PL of monolayer MoS₂ (and WS₂) across its vdW heterojunction with multi-layer SnSe₂ via FRET with single and two-photon excitation. Counteracting the charge transfer across highly staggered conduction bands of MoS₂ and SnSe₂, MoS₂ single-photon luminescence (1P-PL) shows ~14-fold enhancement at room temperature with resonant excitation and ~5-fold enhancement with non-resonant excitation, while two-photon luminescence (2P-PL) of MoS₂ shows up to ~7.5-fold enhancement with non-resonant excitation. Even with the insertion of few-layer hBN between MoS₂ and SnSe₂, the 1P-PL enhancement persists up to 5 times with resonant excitation. We demonstrate modulation of the degree of the PL enhancement by systematic parameter variation, including donor material, acceptor material, their thickness, physical separation between donor and acceptor, sample temperature, and excitation wavelength which corroborate FRET aided PL enhancement. We emphasize the intrinsic advantage of realizing FRET with SnSe₂ as a donor and elucidate the impact of multiple parameters on the luminescence enhancement using rate equation analysis.

Results and Discussions:

FRET allows transitions in the acceptor resonant to the energy of the excited states in the donor. In the approximation of weak coupling, the rate of FRET depends on the spectral overlap between the donor's emission and the acceptor's absorption, the relative orientation of the dipoles across the donor and the acceptor and the physical separation between them.^{23,24} Considering the above factors, we realize FRET across a vdW heterostructure with monolayer MoS₂ (1L-MoS₂) or WS₂ (1L-WS₂) as acceptor, stacked on top of multi-layer SnSe₂ as donor, which acts as a scavenger of

the light unabsorbed by the top monolayer. With vdW stacks of layered materials, FRET benefits from the in-plane orientation of dipoles in both the donor and the acceptor coupled with the closest possible vertical spacing, as depicted in Figure 1a. While SnSe₂ is an indirect bandgap material with an energy gap of 1.1 eV, the choice of SnSe₂ stems from its direct gap at the ‘K’ point^{25–30} which is close to the excitonic gap of 1L-MoS₂³¹ and 1L-WSe₂,³² as shown in Figure 1b. SnSe₂ also exhibits nearly flat bands at the direct gap facilitating strong absorption of light. Due to its indirect nature, we did not obtain any luminescence from SnSe₂, down to 4 K.

Single photon luminescence enhancement: We first perform 1P-PL measurement on the isolated 1L-MoS₂ (denoted as M) and the 1L-MoS₂/SnSe₂ junction (denoted as MS) at room temperature (RT) with resonant (633 nm) and non-resonant (532 nm) single-photon excitations. Illumination of MS region with 532 nm laser, which is non-resonant to both MoS₂ and SnSe₂, creates carriers much above their direct transition, while 633 nm near-resonantly excites both MoS₂ and SnSe₂. Figure 1c shows the PL map (embedded in the optical image) of the MS stack (sample 1, denoted as J1) under 633 nm excitation (See Figure S1a in **Supporting Information** for the optical image). The green dotted line in the image depicts the periphery of 1L-MoS₂ transferred on top of SnSe₂ (orange dotted boundary) using dry transfer method (See **Methods** for heterojunction fabrication and Figure S1b in **Supporting Information** for Raman characterization). PL mapped area covers individual 1L-MoS₂, SnSe₂ and junction regions, and shows strong and uniform enhancement in the junction region. Figure 1d shows a representative PL spectrum of isolated MoS₂ (M-J1) and junction (MS-J1) regions corresponding to the PL map in Figure 1c. Fitting of the above spectra for individual exciton and trion peaks^{17,33} gives about 14 times enhancement for A_{1s} exciton peak of MS-J1. When the excitation wavelength is switched to 532 nm, the PL enhancement persists as shown in Figure 1e but the enhancement of A_{1s} peak goes down to a factor of ~5. On the contrary,

trion (T) peak intensity remains nearly unchanged and B_{1s} peak gets quenched. The strong PL enhancement of the MS region is verified from two other samples, J2 and J3 (See Figure S2 in **Supporting Information**).

Interestingly, the MS junction forms a type-I heterojunction with ~1 eV CB offset, as shown in Figure 1b. The band offsets force fast charge transfer from MoS₂ to SnSe₂,³⁴ which is expected to quench the MoS₂ PL strength significantly, instead of enhancing. Such charge transfer driven PL quenching has been widely reported in the past.^{35–37} The observation of strong PL enhancement despite such charge transfer suggests that SnSe₂ is playing a crucial role in the enhancement mechanism. In order to verify this, we replace SnSe₂ by 1T-TaS₂,^{38,39} a material that exhibits relatively weak light absorption. Figure 1f depicts the PL spectra of isolated 1L-MoS₂ (M-J4) and 1L-MoS₂/TaS₂ (MT-J4) with 633 nm excitation (See Figure S1c in **Supporting Information** for an optical image of junction J4) – clearly indicating quenching of PL in the junction. Also, we observe PL quenching in 1L-MoS₂/graphene, 1L-WSe₂/graphene, and 1L-MoS₂/In_{0.53}Ga_{0.47}As junctions compared to corresponding isolated monolayers, further indicating the crucial role played by SnSe₂ in the observed PL enhancement.

Evidence of FRET mechanism: In order to rule out any inter-layer charge transfer and validate the FRET driven non-radiative energy transfer as the dominant PL enhancement mechanism, a ~10 nm thick hBN film is inserted as a barrier layer between 1L-MoS₂ and SnSe₂, which blocks any possible inter-layer charge transfer. Figure 2a shows the 1L-MoS₂/hBN/SnSe₂ junction (J5) with highlighted boundaries of each layer. The corresponding PL mapping taken across the portions of 1L-MoS₂/hBN (MH-J5) and 1L-MoS₂/hBN/SnSe₂ (MHS-J5) with 633 nm excitation suggests that MoS₂ PL enhances strongly on the latter portion with respect to 1L-MoS₂/hBN. The thickness of the hBN and the SnSe₂ layers can be inferred from the AFM scans along dotted lines

A and B, as shown in the inset. Figure 2b depicts the representative spectra of the different regions of varying SnSe₂ thickness, along the dotted arrow B in Figure 2a. Similar PL enhancement is demonstrated across the MHS region in another sample J6 shown in Figure S3 of **Supporting Information**. These observations corroborate that the PL enhancement is driven by near-field dipolar coupling across 1L-MoS₂/SnSe₂ that exists even in the presence of an energy barrier like hBN.

The second, third and fourth panels of Figure 2b show a systematic reduction of the PL intensity with an increase in the SnSe₂ thickness. While heterojunctions with thin SnSe₂ show PL enhancement, with thicker SnSe₂ (beyond ~20 nm), we observe a consistent quenching of the PL at the junction compared to isolated MoS₂. A similar trend is maintained even when the hBN spacer was removed (see Table 1). Such a systematic variation of PL intensity with the SnSe₂ film thickness provides another direct evidence of FRET as explained below.

Figure 2c shows reflectance contrast spectra of isolated SnSe₂ films with varying thickness placed on SiO₂/Si substrate (see **Methods** for measurement details), measured at room temperature. The dip in the reflectance contrast is found to be efficiently modulated by the thickness of SnSe₂. Note that this dip is spectrally broad and does not show any sharp excitonic feature (even down to 4 K, see Figure S4 in **Supporting Information**). This is in agreement with our previous KPFM measurements which show that the SnSe₂ is degenerately n-doped with the Fermi level about 0.3 eV above conduction band (CB) minimum.⁴⁰ The screening offered by the large carrier concentration suppresses strongly bound exciton state in SnSe₂. Throughout this paper, we thus assume that the transition dipole in SnSe₂ is governed by free electron-hole pairs.

The absorption peaks corresponding to the minima in the reflectance contrast spectra are plotted in Figure 2d as a function of SnSe₂ thickness. In the same plot, we also show the A_{1s} excitonic

absorption peaks of monolayers of MoS₂, WS₂ and WSe₂, at room temperature. Along with the spectral overlap between the donor and the acceptor, strength of absorption in the donor is an important parameter that controls the efficiency of energy transfer through FRET process. The diagram suggests that by changing the thickness of SnSe₂ film, one can effectively tune the strength of absorption at corresponding direct gap in SnSe₂ (donor) and the spectral overlap between SnSe₂ (donor) and the monolayer acceptor, in turn controlling the non-radiative energy transfer efficiency. In particular, as the thickness of SnSe₂ film is increased beyond ~20 nm, the FRET efficiency is reduced between SnSe₂ direct gap absorption and the MoS₂ A_{1s} excitonic absorption peak, and is in excellent agreement with our PL data.

In agreement with the above argument, replacing 1L-MoS₂ by 1L-WS₂ (with a 2.02 eV excitonic gap at RT) yields a strong PL enhancement as well. This is shown by the PL mapping image of the WS₂/SnSe₂ stack J7 in Figure 2e (See Figure S1d in **Supporting Information** for its optical image). We obtain ~3 times enhancement (with off-resonant 532 nm excitation) of WS₂ PL on the junction with thin SnSe₂ (region A) and the enhancement goes down when SnSe₂ becomes thicker (region B and C). A representative spectrum is shown in the middle panel of Figure 2f. In contrast, when the resonance between monolayer TMD and SnSe₂ is avoided by using 1L-WSe₂/SnSe₂ junction J8, where excitonic gap of WSe₂ (~1.65 eV at RT) is much below the SnSe₂ direct gap,³² no PL enhancement is observed, as seen from the right most panel of Figure 2f.

Further, we observe a strong temperature dependence of the PL enhancement factor on the MS junction region. Figure 3a and 3b show the corresponding spectra of M-J2 and MS-J2 under 633 nm and 532 nm excitations, up to 200 K. In both the cases, the ratio (α) of the peak intensity on the junction to that on the 1L-MoS₂ of both exciton (A_{1s}) and trion increase with temperature. At low temperatures below 100K, MoS₂ PL intensity on the junction is reduced drastically for both

A_{1s} and trion peaks. Above 100K, while the trion peak remains quenched on the junction, the A_{1s} peak sharply increases with temperature. Figure 3c depicts the temperature variation of α for A_{1s} and trion of 1L-MoS₂/SnSe₂ (MS-J2) under 532 nm excitation. Similar temperature dependence of α for A_{1s} is also seen on 2L-MoS₂/SnSe₂ junction where the degree of quenching increases with a reduction in the temperature (See Figure S5 in **Supporting Information**). As explained in Figure S6b of **Supporting Information**, such a strong dependence on temperature⁴¹ can be directly correlated with a temperature dependent rate of the non-radiative inter-layer energy transfer. Figure 3c also illustrates the variation of α with temperature for A_{1s} on 1L-MoS₂/TaS₂ (MT-J4) under 633 nm excitation, which, on the contrary, does not show any temperature dependence of the degree of PL quenching, unlike MoS₂/SnSe₂ junction.

Other possible mechanisms as play: Constructive interference with the back-reflected light from the substrate is one mechanism often used to enhance the PL strength. Two experimental observations also help us to rule out the contribution of interference effect in PL enhancement.. First, as mentioned above, the PL enhancement at the MoS₂/SnSe₂ junction shows a strong temperature dependence. Any such constructive interference with back reflected light is not expected to be a strong function of sample temperature. Second, we observe a strong quenching of the MoS₂ Raman peaks at the MoS₂/SnSe₂ junction (See Figure S1b in **Supporting Information**) while the PL intensity is enhanced. Any optical effect like constructive interference would be similar for both these cases, indicating a different origin for PL enhancement. Raman peaks are strongly quenched since the carrier scattering with optical phonons is a relatively slower process compared to ultra-fast inter-layer charge and energy transfer.

Another possible mechanism could be enhanced quantum yield at the heterojunction due to isolation from SiO₂ trap induced inhomogeneity. While such inhomogeneities can play an

important role at low temperature, exciton-phonon scattering plays a dominant role at room temperature.⁴² The observation of strong PL enhancement at room temperature thus indicates a relatively small effect of changes in quantum yield. In addition, any such enhanced quantum yield cannot explain the SnSe₂ thickness dependence of the PL strength at the heterojunction in Figure 2a-b, since in all these cases, 1L-MoS₂ is sitting on top of hBN/SnSe₂ stack, hence the quantum yield is expected to be similar.

Modeling the processes using rate equations: In Table 1, we summarize the experimental observations over different stacks, and dependence of PL strength on excitation wavelength (resonant versus non-resonant), sample temperature, donor and acceptor materials, thickness of the donor and the acceptor, and the separation between them. We now derive an expression for the PL enhancement factor (α) from a rate equation analysis which provides an insight into the effect of various parameters on α . The different processes occurring across MoS₂, SnSe₂ and the junction on illumination are represented in the transition picture with resonant excitation in Figure 4a. Γ_r and Γ_{nr} are respectively the radiative and non-radiative decay rates of exciton in MoS₂, while Γ_s is the scattering rate of transition dipoles in SnSe₂. Let Γ_{CT}^{M-S} and Γ_{ET}^{M-S} denote the rate of charge and energy transfer respectively from MoS₂ to SnSe₂. The corresponding energy transfer rate from SnSe₂ to MoS₂ is denoted by Γ_{ET}^{S-M} . The detailed analysis of the rate equations in MoS₂ and the junction considering all the relevant processes as indicated in Figure 4a is presented in **Supporting Information**. α is deduced as

$$\alpha = \left(\frac{G_{e-h}^S}{G_{ex}^M} \right) \frac{\gamma}{\gamma + \beta} \quad (1)$$

where $\gamma = \frac{\Gamma_{ET}^{S-M}}{\Gamma_S}$, $\beta = 1 + \left(\frac{\Gamma_{CT}^{M-S} + \Gamma_{ET}^{M-S}}{\Gamma_r + \Gamma_{nr}^M} \right)$, G_{e-h}^S is the effective rate of generation of transition dipoles in SnSe₂ at the energy states resonant to A_{1s} excitonic states of MoS₂ and G_{ex}^M is the effective rate of generation of excitons in MoS₂. γ represents the ratio of the rate of resonant energy transfer from SnSe₂ to MoS₂, to the relaxation rate to the indirect band within SnSe₂. A large value of γ is desirable, which is achieved by the ultra-fast inter-layer energy transfer rates in vdW heterostructures as theoretically predicted in literature.^{22,36,43,44} Clearly, α takes a maximum value of $\frac{G_{e-h}^S}{G_{ex}^M}$ when $\beta \ll \gamma$.

Resonant and non-resonant excitations of 1L-MoS₂/SnSe₂ differ in the factor $\frac{G_{e-h}^S}{G_{ex}^M}$ that changes α in (1). As non-resonant excitation creates e-h pairs in MoS₂ and SnSe₂ at much higher energies above the direct transitions, scattering of these hot carriers lowers both G_{e-h}^S and G_{ex}^M . Also, as few-layer hBN is inserted between 1L-MoS₂ and SnSe₂, Γ_{CT}^{M-S} is completely suppressed, however, coupled with a reduction in Γ_{ET}^{M-S} due to increased separation (d).⁴¹ This effectively results in a lower value of α at 1L-MoS₂/hBN/SnSe₂ junction than that of 1L-MoS₂/SnSe₂ junction.

The dissimilarity in the degree of enhancement for A_{1s} exciton and trion can be explained with the competition between Γ_r and the rate of FRET as elucidated in Figure S6c of **Supporting Information**. As A_{1s} exciton exhibits faster radiative decay (Γ_r), PL enhancement persists despite the intrinsic charge (Γ_{CT}^{M-S}) and energy (Γ_{ET}^{M-S}) transfer from MoS₂ to SnSe₂. On the other hand, trions possess slower Γ_r ⁸ and hence suffer from Γ_{CT}^{M-S} and Γ_{ET}^{M-S} because of their longer lifetime. This effectively increases β in (3) resulting in suppressed or no enhancement for the trion. This points to the significance of the oscillator strength of transition dipoles in the acceptor for efficient FRET induced PL enhancement.

Efficient FRET due to additional degree of freedom in SnSe₂: From a microscopic point of view, energy and center of mass (COM) momentum must be conserved between the donor and the acceptor dipoles during the FRET process.⁴¹ The layered heterostructure forces the dipoles to be oriented in the plane, facilitating the conservation of the in-plane momentum, as illustrated in Figure 1a. Since there is a mismatch (ΔE_g) between the direct bandgap in SnSe₂ and exciton gap in 1L-MoS₂, coupled with a mismatch in the effective mass values in these materials, it is difficult to conserve both energy and momentum simultaneously when it comes to exciton-exciton energy transfer, as pointed out by Lyo.⁴¹ To this end, the transition dipoles in SnSe₂ being governed by e-h pair as explained earlier (and not strongly bound exciton due to screening), allows an additional degree of freedom in the form of the relative motion between the electron and the hole.

The situation is schematically illustrated in Figure 4b. The violet color band on the left is the exciton band structure of MoS₂, with the energy given by $E = \frac{\hbar^2 K_m^2}{2M_m}$, where \mathbf{K}_m is the COM momentum of the MoS₂ exciton, and $M_m = m_{e,MoS_2} + m_{h,MoS_2}$. In SnSe₂, the total energy of the e-h pair is given by the sum of the COM component (in orange) and the relative component (in blue): $E = \frac{\hbar^2 K_s^2}{2M_s} + \frac{\hbar^2 k_s^2}{2\mu_s}$ where \mathbf{K}_s is the in-plane COM momentum, \mathbf{k}_s is the relative part of the in-plane momentum, and $\mu_s = \frac{m_{e,SnSe_2} m_{h,SnSe_2}}{M_s}$ is the reduced mass, with $M_s = m_{e,SnSe_2} + m_{h,SnSe_2}$.

Energy conservation during FRET at a COM momentum $\mathbf{K}_m = \mathbf{K}_s = \mathbf{K}_0$ yields

$$\frac{\hbar^2 K_0^2}{2M_m} = \Delta E_g + \frac{\hbar^2 K_0^2}{2M_s} + \frac{\hbar^2 k_s^2}{2\mu_s} \quad (2)$$

Equation (2) clearly shows that the free variable k_s due to the relative movement between electron and hole in SnSe₂ relaxes the simultaneous energy-momentum conservation condition, improving the FRET efficiency. For a given K_0 , we have

$$k_s = \frac{2\mu_s}{\hbar^2} \sqrt{\frac{\hbar^2 K_0^2}{2} \left(\frac{1}{M_m} - \frac{1}{M_s} \right) - \Delta E_g} \quad (3)$$

where solutions exist for k_s if $\left[\frac{\hbar^2 K_0^2}{2} \left(\frac{1}{M_m} - \frac{1}{M_s} \right) - \Delta E_g \right] > 0$. In the present case, we have $M_m < M_s$, and $\Delta E_g > 0$. Also, note that equation (2) only has a constraint on the absolute value k_s , hence all possible angular directions in the plane of the layer can contribute to FRET, as illustrated in Figure 4b.

PL enhancement with two-photon excitation: We now show the generic nature of the proposed method by demonstrating enhanced luminescence using two-photon absorption (TPA). TPA is a third order non-linear process where excitation is performed with two photons of longer wavelength compared to the bandgap. TPA in materials with optical band gap in the visible range is attractive for dual mode visible-IR photodetection.⁴⁵ TPA is useful to access the energy states such as dark excitons which are forbidden by selection rules under single-photon excitation.^{46,47} Two-photon luminescence (2P-PL) is also widely sought in biological sensing and high-resolution imaging due to axial localization and large penetration depth.⁴⁸ The FRET process across layered heterostructures is a very versatile method of energy transfer that is applicable to two-photon absorption as well. This allows facile integration of a material with strong TPA as a donor layer with a highly luminescent medium like TMD monolayer, as an acceptor, and is promising for such imaging and spectroscopic applications.^{49,50} Such mechanism can also yield enhanced frequency up-conversion. Recent reports have shown utilization of donors with higher two-photon absorption cross-section to yield higher 2P-PL.^{51,52}

We explore this phenomenon across 1L-MoS₂/SnSe₂ (sample J1) by two-photon PL imaging using 1040 nm excitation (See **Methods**). We observe a 7.5-fold 2P-PL enhancement as shown in the 2P-PL map of J1 in Figure 5a where the emitted light is filtered at 650 nm with a band pass window

of 40 nm. Figure 5b shows the voltage signal of the PMT that detects 2P-PL from the isolated 1L-MoS₂ (violet) and the junction (orange) as a function of peak irradiance. The enhancement is particularly strong at lower peak irradiance, which is generally desirable to obtain strong 2P-PL without possible sample damage. The 2P-PL signal from the isolated 1L-MoS₂ portion shows non-linear variation with peak irradiance. On the other hand, 2P-PL from the heterojunction, while showing strong enhancement compared to the isolated MoS₂ portion, does not exhibit any such non-linearity in the measured range. This suggests that 1L-MoS₂ on the junction gets excited by the cascaded process of TPA in SnSe₂ followed by carrier relaxation and subsequent FRET from SnSe₂ to MoS₂, as schematically depicted in Figure 5c. Such 2P-PL enhancement is also observed across the 1L-MoS₂/hBN/SnSe₂ junction. Thus, FRET with two-photon excitation can aid to increase the saturation threshold of TPA in TMD monolayer besides enhancing 2P-PL significantly at lower power levels. This way of enhancing the luminescence with multi-photon excitation across layered heterostructures is interesting for nanoscale photonic applications.⁹

Conclusion:

In summary, using a layered heterostructure of monolayer TMD and multi-layer SnSe₂, we demonstrated a strongly enhanced luminescence manifested through non-radiative resonance energy transfer. This mechanism benefits from the following factors: 1) nanometer scale separation between the donor and the acceptor layer; 2) in-plane orientation of dipoles, both in the donor and the acceptor, providing improved dipolar coupling; 3) scavenging of light that is unabsorbed by monolayer TMD using multi-layer SnSe₂ which also has a near-resonant direct transition to exciton state of the corresponding TMD; 4) energy transfer from free e-h pairs in SnSe₂ to strongly bound excitons in monolayer TMD relaxing energy conservation due to additional degree of freedom. The generic nature of the mechanism is attractive, and is demonstrated for both single- and two-

photon luminescence enhancement. The luminescence enhancement being uniform across the entire overlapped junction area is advantageous over the local enhancement in plasmonic structure or QD coupled 2D layers. The general strategy of combining a weak absorber, but highly luminescent material (like monolayer TMD) with a strong optical absorber devoid of luminescence (like SnSe₂) can be extended to other material systems as well, and holds promise for improved quantum efficiency in multiple applications such as biomedical imaging, light emitting diode, light harvesting, and non-linear spectroscopy. Also, in order to further improve the overall photoluminescence from monolayer TMDs, the scheme presented here can work in tandem with other techniques (for example, defect passivation¹⁸) that help to improve the quantum yield in the monolayer.

Methods:

Fabrication of heterojunction: MoS₂/SnSe₂ stack is prepared by all-dry transfer method using visco-elastic stamping maneuvered by micromanipulator. First, SnSe₂ is exfoliated on to 285 nm SiO₂ coated Si substrate. MoS₂ is exfoliated on PDMS attached to a glass slide and the MoS₂ flake of desired thickness is identified and then transferred on top of multi-layer SnSe₂ flake of interest. After transfer, MoS₂/SnSe₂ stack is measured without any annealing. However, remeasurements after heating the stack did not differ significantly with the measurements of pre-heated stack.

Reflectance contrast measurement: For reflectance contrast measurements, SnSe₂ flakes of varying thickness are exfoliated on top of 285 nm SiO₂ coated Si substrate. Thickness of SnSe₂ flakes is determined with Atomic Force Microscopy. A broadband radiation is passed through a pinhole and focused on to the SnSe₂ flake of interest using 100x objective. The reflected light is collected in a confocal mode using a spectrometer with 1800 lines per mm grating and CCD. Reflectance spectrum from the bare SiO₂ substrate (R_{SiO_2}) is subtracted from the reflectance

spectrum of individual SnSe₂ flake (R_{Sample}) and normalized with R_{SiO_2} to identify the absorption energy position of SnSe₂. Reflectance contrast measurements at 4K are taken in a similar way as above using a 50x objective to focus the light on to the sample in a closed-cycle cryostat.

Two photon PL microscopy: The two photon PL imaging of the hetero junction is performed using a fiber laser source (Coherent Fidelity HP-10) operating at 1040 nm wavelength with 80 MHz repetition rate. The horizontally polarized laser of 140 fs pulse width is focused onto the sample using a ~20x/0.75 objective (Olympus UPLSAPO 20x). The two-photon PL signal is collected using the same objective and then separated from the excitation beam using a dichroic mirror and detected using a photomultiplier tube (Hamamatsu R3896). A 650 nm/40 nm band-pass filter in combination with an 890 nm short-pass filter is mounted in front of the photomultiplier tube for efficient rejection of any residual excitation beam and to minimize the background signal. Two-photon PL images are acquired by scanning a pair of galvanometric mirrors (Thorlabs GVS002) over an imaging area of 15 μm x 15 μm .

Acknowledgements:

K. M. acknowledges the support a grant from Indian Space Research Organization (ISRO), grants under Ramanujan Fellowship, Early Career Award, and Nano Mission from the Department of Science and Technology (DST), Government of India, and support from MHRD, MeitY and DST Nano Mission through NNetRA.

Conflicts of Interest:

The authors declare no financial or non-financial conflict of interest.

References:

- (1) Splendiani, A.; Sun, L.; Zhang, Y.; Li, T.; Kim, J.; Chim, C. Y.; Galli, G.; Wang, F. Emerging Photoluminescence in Monolayer MoS₂. *Nano Lett.* **2010**, *10*, 1271–1275.
- (2) He, K.; Kumar, N.; Zhao, L.; Wang, Z.; Mak, K. F.; Zhao, H.; Shan, J. Tightly Bound Excitons in Monolayer WSe₂. *Phys. Rev. Lett.* **2014**, *113*, 026803.
- (3) Ugeda, M. M.; Bradley, A. J.; Shi, S. F.; Da Jornada, F. H.; Zhang, Y.; Qiu, D. Y.; Ruan, W.; Mo, S. K.; Hussain, Z.; Shen, Z. X.; Wang, F.; Louie, S. G.; Crommie, M. F. Giant Bandgap Renormalization and Excitonic Effects in a Monolayer Transition Metal Dichalcogenide Semiconductor. *Nat. Mater.* **2014**, *13*, 1091–1095.
- (4) Wang, G.; Chernikov, A.; Glazov, M. M.; Heinz, T. F.; Marie, X.; Amand, T.; Urbaszek, B. Colloquium: Excitons in Atomically Thin Transition Metal Dichalcogenides. *Rev. Mod. Phys.* **2018**, *90*, 21001.
- (5) Poellmann, C.; Steinleitner, P.; Leierseder, U.; Nagler, P.; Plechinger, G.; Porer, M.; Bratschitsch, R.; Schüller, C.; Korn, T.; Huber, R. Resonant Internal Quantum Transitions

- and Femtosecond Radiative Decay of Excitons in Monolayer WSe₂. *Nat. Mater.* **2015**, *14*, 889–893.
- (6) Palummo, M.; Bernardi, M.; Grossman, J. C. Exciton Radiative Lifetimes in Two-Dimensional Transition Metal Dichalcogenides. *Nano Lett.* **2015**, *15*, 2794–2800.
- (7) Robert, C.; Lagarde, D.; Cadiz, F.; Wang, G.; Lassagne, B.; Amand, T.; Balocchi, A.; Renucci, P.; Tongay, S.; Urbaszek, B.; Marie, X. Exciton Radiative Lifetime in Transition Metal Dichalcogenide Monolayers. *Phys. Rev. B* **2016**, *93*, 20543.
- (8) Wang, H.; Zhang, C.; Chan, W.; Manolatou, C.; Tiwari, S.; Rana, F. Radiative Lifetimes of Excitons and Trions in Monolayers of the Metal Dichalcogenide MoS₂. *Phys. Rev. B* **2016**, *93*, 045407.
- (9) Autere, A.; Jussila, H.; Dai, Y.; Wang, Y.; Lipsanen, H.; Sun, Z. Nonlinear Optics with 2D Layered Materials. *Adv. Mater.* **2018**, *30*, 1705963.
- (10) Bernardi, M.; Palummo, M.; Grossman, J. C. Extraordinary Sunlight Absorption and One Nanometer Thick Photovoltaics Using Two-Dimensional Monolayer Materials. *Nano Lett.* **2013**, *13*, 3664–3670.
- (11) Janisch, C.; Song, H.; Zhou, C.; Lin, Z.; Elías, A. L.; Ji, D.; Terrones, M.; Gan, Q.; Liu, Z. MoS₂ Monolayers on Nanocavities: Enhancement in Light–matter Interaction. *2D Mater.* **2016**, *3*, 025017.
- (12) Noori, Y. J.; Cao, Y.; Roberts, J.; Woodhead, C.; Bernardo-Gavito, R.; Tovee, P.; Young, R. J. Photonic Crystals for Enhanced Light Extraction from 2D Materials. *ACS Photonics* **2016**, *3*, 2515–2520.

- (13) Bahauddin, S. M.; Robotjazi, H.; Thomann, I. Broadband Absorption Engineering to Enhance Light Absorption in Monolayer MoS₂. *ACS Photonics* **2016**, *3*, 853–862.
- (14) Liu, J. T.; Wang, T. B.; Li, X. J.; Liu, N. H. Enhanced Absorption of Monolayer MoS₂ with Resonant Back Reflector. *J. Appl. Phys.* **2014**, *115*.
- (15) Wang, Z.; Dong, Z.; Gu, Y.; Chang, Y. H.; Zhang, L.; Li, L. J.; Zhao, W.; Eda, G.; Zhang, W.; Grinblat, G.; Maier, S. A.; Yang, J. K. W.; Qiu, C. W.; Wee, A. T. S. Giant Photoluminescence Enhancement in Tungsten-Diselenide-Gold Plasmonic Hybrid Structures. *Nat. Commun.* **2016**, *7*, 11283.
- (16) Sun, J.; Hu, H.; Zheng, D.; Zhang, D.; Deng, Q.; Zhang, S.; Xu, H. Light-Emitting Plexciton: Exploiting Plasmon-Exciton Interaction in the Intermediate Coupling Regime. *ACS Nano* **2018**, *12*, 10393–10402.
- (17) Mouri, S.; Miyauchi, Y.; Matsuda, K. Tunable Photoluminescence of Monolayer MoS₂ via Chemical Doping. *Nano Lett.* **2013**, *13*, 5944–5948.
- (18) KC, S.; Zhang, X.; Ager, J. W.; Madhvapathy, S. R.; Lee, S.-C.; Azcatl, A.; Addou, R.; Yablonovitch, E.; Javey, A.; Lien, D.-H.; Noh, J.; Xiao, J.; Dubey, M.; Kiriya, D.; Amani, M.; Cho, K.; Wallace, R. M.; He, J.-H. Near-Unity Photoluminescence Quantum Yield in MoS₂. *Science*. **2015**, *350*, 1065–1068.
- (19) Guzelturk, B.; Demir, H. V. Near-Field Energy Transfer Using Nanoemitters For Optoelectronics. *Adv. Funct. Mater.* **2016**, *26*, 8158–8177.
- (20) Medintz, I. L.; Hildebrandt, N. *FRET-Förster Resonance Energy Transfer: From Theory to Applications*; John Wiley & Sons, 2013.

- (21) Gu, J.; Liu, X.; Lin, E. C.; Lee, Y. H.; Forrest, S. R.; Menon, V. M. Dipole-Aligned Energy Transfer between Excitons in Two-Dimensional Transition Metal Dichalcogenide and Organic Semiconductor. *ACS Photonics* **2018**, *5*, 100–104.
- (22) Kozawa, D.; Carvalho, A.; Verzhbitskiy, I.; Giustiniano, F.; Miyauchi, Y.; Mouri, S.; Castro Neto, A. H.; Matsuda, K.; Eda, G. Evidence for Fast Interlayer Energy Transfer in MoSe₂/WS₂ Heterostructures. *Nano Lett.* **2016**, *16*, 4087–4093.
- (23) Scholes, G. D. Long-Range Resonance Energy Transfer In Molecular Systems. *Annu. Rev. Phys. Chem.* **2003**, *54*, 57–87.
- (24) Basko, D.; La Rocca, G. C.; Bassani, F.; Agranovich, V. M. Förster Energy Transfer from a Semiconductor Quantum Well to an Organic Material Overlayer. *Eur. Phys. J. B - Condens. Matter Complex Syst.* **1999**, *8*, 353–362.
- (25) Evans, B. L.; Hazelwood, R. A. Optical and Electrical Properties of SnSe₂. *J. Phys. D. Appl. Phys.* **1969**, *2*, 1507.
- (26) Murray, R. B.; Williams, R. H. Band Structure and Photoemission Studies of SnS₂ and SnSe₂. II. Theoretical. *J. Phys. C Solid State Phys.* **1973**, *6*, 3643.
- (27) Garg, A. K.; Agnihotri, O. P.; Jain, A. K.; Tyagi, R. C. Optical Absorption Spectrum of Tin Diselenide Single Crystals. *J. Appl. Phys.* **1976**, *47*, 997–1000.
- (28) El-Nahass, M. M. Optical Properties of Tin Diselenide Films. *J. Mater. Sci.* **1992**, *27*, 6597–6604.
- (29) Manou, P.; Kalomiros, J. A.; Anagnostopoulos, A. N.; Kambas, K. Optical Properties of SnSe₂ Single Crystals. *Mater. Res. Bull.* **1996**, *31*, 1407–1415.

- (30) Brebner, J. L.; Perluzzo, G. Thermoreflectance Measurements on SnS₂ and SnSe₂. *Can. J. Phys.* **1982**, *60*, 915–918.
- (31) Mak, K. F.; Lee, C.; Hone, J.; Shan, J.; Heinz, T. F. Atomically Thin MoS₂: A New Direct-Gap Semiconductor. *Phys. Rev. Lett.* **2010**, *105*, 136805.
- (32) Zhao, W.; Ghorannevis, Z.; Chu, L.; Toh, M.; Kloc, C.; Tan, P.-H.; Eda, G. Evolution of Electronic Structure in Atomically Thin Sheets of WS₂ and WSe₂. *ACS Nano* **2012**, *7*, 791–797.
- (33) Lee, H. S.; Kim, M. S.; Kim, H.; Lee, Y. H. Identifying Multiexcitons in MoS₂ Monolayers at Room Temperature. *Phys. Rev. B* **2016**, *93*, 140409.
- (34) Zhou, X.; Zhou, N.; Li, C.; Song, H.; Zhang, Q.; Hu, X.; Gan, L.; Li, H.; Lü, J.; Luo, J.; Xiong, J.; Zhai, T. Vertical Heterostructures Based on SnSe₂/MoS₂ for High Performance Photodetectors. *2D Mater.* **2017**, *4*, 025048.
- (35) Murali, K.; Dandu, M.; Das, S.; Majumdar, K. Gate-Tunable WSe₂/SnSe₂ Backward Diode with Ultrahigh-Reverse Rectification Ratio. *ACS Appl. Mater. Interfaces* **2018**, *10*, 5657–5664.
- (36) Hill, H. M.; Rigosi, A. F.; Raja, A.; Chernikov, A.; Roquelet, C.; Heinz, T. F. Exciton Broadening in WS₂/Graphene Heterostructures. *Phys. Rev. B* **2017**, *96*, 205401.
- (37) Hong, X.; Kim, J.; Shi, S.; Zhang, Y.; Jin, C.; Sun, Y.; Tongay, S.; Wu, J.; Zhang, Y.; Wang, F. Ultrafast Charge Transfer in Atomically Thin MoS₂/WS₂ Heterostructures. *Nat. Nanotechnol.* **2014**, *9*, 682–686.
- (38) Barker, A. S.; Ditzenberger, J. A.; DiSalvo, F. J. Infrared Study of the Electronic

- Instabilities in Tantalum Disulfide and Tantalum Diselenide. *Phys. Rev. B* **1975**, *12*, 2049–2054.
- (39) Mehak, M.; Krishna, M.; Nikhil, K.; Kausik, M. Gate-Controlled Large Resistance Switching Driven by Charge-Density Wave in 1T-TaS₂/2H-MoS₂ Heterojunctions. *Phys. Rev. Appl.* **2019**, *10*, 024031.
- (40) Krishna, M.; Kallatt, S.; Majumdar, K. Substrate Effects in High Gain, Low Operating Voltage SnSe₂ Photoconductor. *Nanotechnology* **2018**, *29*, 035205.
- (41) Lyo, S. K. Energy Transfer of Excitons between Quantum Wells Separated by a Wide Barrier. *Phys. Rev. B - Condens. Matter Mater. Phys.* **2000**, *62*, 13641–13656.
- (42) Gupta, G.; Majumdar, K. On the Fundamental Exciton Linewidth Broadening in Monolayer Transition Metal Dichalcogenides. *Phys. Rev. B* **2019**, *99*, 085412.
- (43) Manolatou, C.; Wang, H.; Chan, W.; Tiwari, S.; Rana, F. Radiative and Nonradiative Exciton Energy Transfer in Monolayers of Two-Dimensional Group-VI Transition Metal Dichalcogenides. *Phys. Rev. B* **2016**, *93*, 155422.
- (44) Selig, M.; Malic, E.; Ahn, K. J.; Koch, N.; Knorr, A. Theory of Optically Induced Förster Coupling in van Der Waals Coupled Heterostructures. *Phys. Rev. B* **2019**, *99*, 035420.
- (45) Song, J.; Cui, Q.; Li, J.; Xu, J.; Wang, Y.; Xu, L.; Xue, J.; Dong, Y.; Tian, T.; Sun, H.; Zeng, H. Ultralarge All-Inorganic Perovskite Bulk Single Crystal for High-Performance Visible–Infrared Dual-Modal Photodetectors. *Adv. Opt. Mater.* **2017**, *5*, 1700157.
- (46) Ye, Z.; Cao, T.; O’Brien, K.; Zhu, H.; Yin, X.; Wang, Y.; Louie, S. G.; Zhang, X. Probing Excitonic Dark States in Single-Layer Tungsten Disulphide. *Nature* **2014**, *513*, 214–218.

- (47) Berkelbach, T. C.; Hybertsen, M. S.; Reichman, D. R. Bright and Dark Singlet Excitons via Linear and Two-Photon Spectroscopy in Monolayer Transition-Metal Dichalcogenides. *Phys. Rev. B - Condens. Matter Mater. Phys.* **2015**, *92*, 085413.
- (48) Zipfel, W. R.; Williams, R. M.; Webb, W. W. Nonlinear Magic: Multiphoton Microscopy in the Biosciences. *Nat. Biotechnol.* **2003**, *21*, 1369–1377.
- (49) Brousmiche, D. W.; Serin, J. M.; Fréchet, J. M. J.; He, G. S.; Lin, T. C.; Chung, S. J.; Prasad, P. N. Fluorescence Resonance Energy Transfer in a Novel Two-Photon Absorbing System. *J. Am. Chem. Soc.* **2003**, *125*, 1448–1449.
- (50) Clapp, A. R.; Pons, T.; Medintz, I. L.; Delehanty, J. B.; Melinger, J. S.; Tiefenbrunn, T.; Dawson, P. E.; Fisher, B. R.; O'Rourke, B.; Mattoussi, H. Two-Photon Excitation of Quantum-Dot-Based Fluorescence Resonance Energy Transfer and Its Applications. *Adv. Mater.* **2007**, *19*, 1921–1926.
- (51) Liu, Q.; Guo, B.; Rao, Z.; Zhang, B.; Gong, J. R. Strong Two-Photon-Induced Fluorescence from Photostable, Biocompatible Nitrogen-Doped Graphene Quantum Dots for Cellular and Deep-Tissue Imaging. *Nano Lett.* **2013**, *13*, 2436–2441.
- (52) Sweet, C.; Pramanik, A.; Jones, S.; Ray, P. C. Two-Photon Fluorescent Molybdenum Disulfide Dots for Targeted Prostate Cancer Imaging in the Biological II Window. *ACS Omega* **2017**, *2*, 1826–1835.

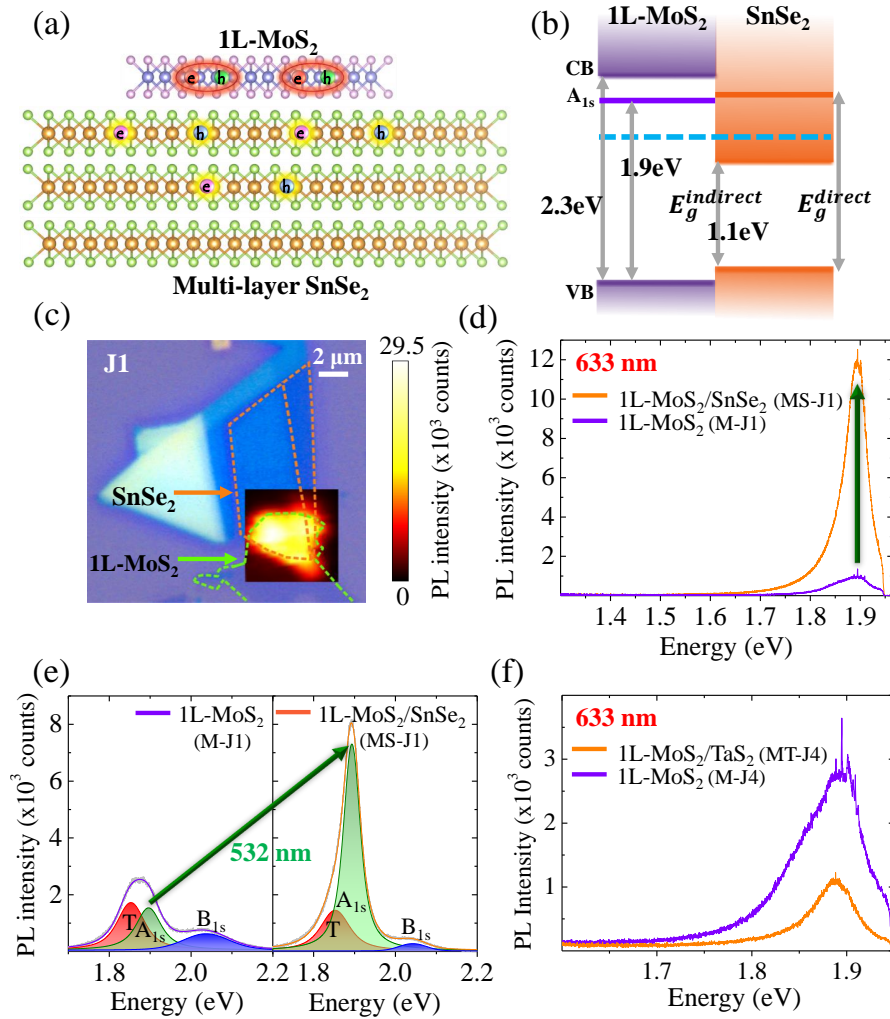


Figure 1: Single-photon luminescence enhancement of 1L-MoS₂ on SnSe₂ at room temperature.

(a) In-plane orientation of dipoles across layered heterostructure which can maximize the efficiency of FRET. (b) Band diagram of 1L-MoS₂/SnSe₂ junction showing type-I heterojunction. In MoS₂, the 1s state of the A exciton (A_{1s}) and the continuum are around 1.9 eV and 2.3 eV. The direct and indirect energy gaps in SnSe₂ are also shown. (c) Optical image of the 1L-MoS₂/SnSe₂ junction (sample J1) with embedded PL map at 1.89 eV under 633 nm excitation at room temperature. Regions highlighted with orange and green dotted lines represent SnSe₂ and 1L-MoS₂, respectively. Color bar maps the PL intensity counts. (d) PL spectra from isolated 1L-MoS₂ on SiO₂ (violet) and 1L-MoS₂/SnSe₂ (orange) of sample J1 under illumination with 633 nm laser. (e) PL spectra from isolated 1L-MoS₂ on SiO₂ (left panel) and 1L-MoS₂/SnSe₂ (right panel) of sample J1 under 532 nm excitation shown along with fitting of corresponding trion (T) and 1s exciton (A_{1s} and B_{1s}) peaks. Grey shaded line represents raw spectral data. (f) PL spectra obtained with 633 nm excitation from isolated 1L-MoS₂ on SiO₂ (violet) and 1L-MoS₂/TaS₂ junction (orange) of sample J4.

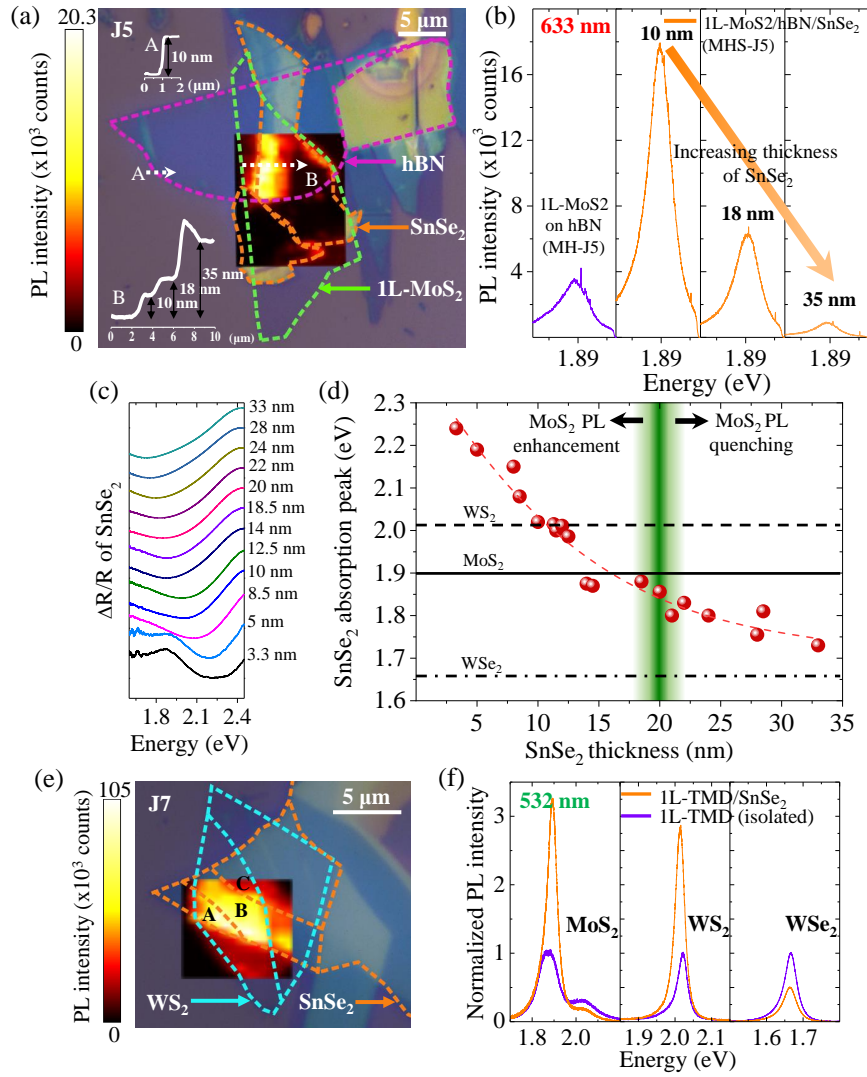


Figure 2: Evidence of FRET mechanism. (a) 1L-MoS₂/hBN/SnSe₂ junction (sample J5) with its optical image and PL map under 633 nm illumination. 1L-MoS₂ (green), hBN (magenta) and SnSe₂ (orange) layers are individually highlighted in the optical image. Thickness of hBN (top inset) and SnSe₂ (bottom inset) layers determined from the step heights in AFM scans along the lines A and B, respectively. (b) PL spectra of 1L-MoS₂/hBN (in violet, left column) and 1L-MoS₂/hBN/SnSe₂ (in orange) with different thickness values of SnSe₂ from sample J5 [along the white dashed arrow B in (a)]. PL intensity of 1L-MoS₂ on the junction decreases with increase in SnSe₂ thickness. (c) Reflectance contrast $\frac{\Delta R}{R} = \frac{R_{SnSe_2} - R_{SiO_2}}{R_{SiO_2}}$ of isolated SnSe₂ on SiO₂ at room temperature. Corresponding thickness of SnSe₂ is indicated adjacent to each spectrum. (d) Absorption peak of SnSe₂ extracted from reflectance contrast as a function of its thickness. The solid, dashed and dot-dashed lines highlight the excitonic resonances of MoS₂, WS₂ and WSe₂ at room temperature. The green gradient line partitions the SnSe₂ thickness regions for MoS₂ PL enhancement and quenching as observed experimentally. (e) Optical image of the 1L-WS₂/SnSe₂ junction (sample J7) with embedded PL map at 2.02 eV under 532 nm excitation at room temperature. Orange and blue dotted lines highlight the portions of SnSe₂ and WS₂, respectively. Region A, B and C represent the WS₂/SnSe₂ regions with increasing SnSe₂ thickness. (f) PL spectra from isolated 1L-TMD on SiO₂ (violet) and 1L-TMD/SnSe₂ junction (orange) of samples J1 (MoS₂/SnSe₂), J7 (WS₂/SnSe₂) and J8 (WSe₂/SnSe₂) with 532 nm excitation.

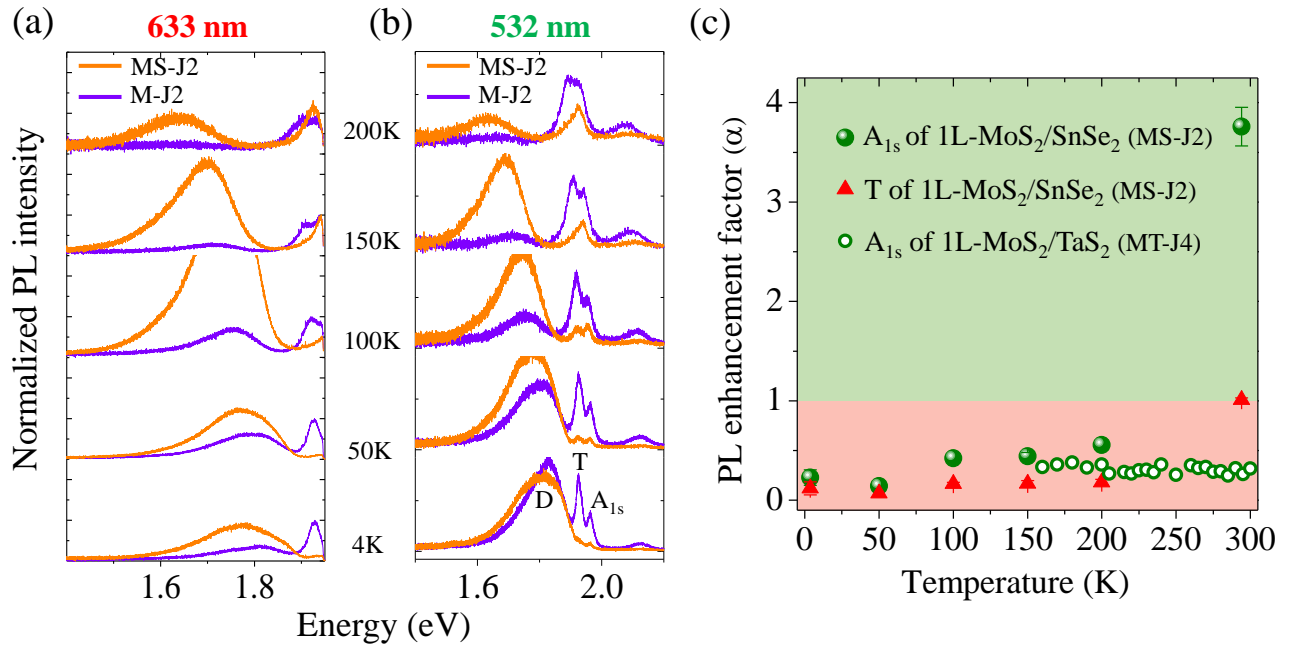


Figure 3: Temperature dependence of PL enhancement. (a-b) PL spectra from isolated 1L-MoS₂ on SiO₂ (violet) and 1L-MoS₂/SnSe₂ (orange) of sample J2 at multiple temperatures with (a) 633 nm and (b) 532 nm excitation respectively. PL spectra are normalized with respect to the maximum PL intensity from isolated 1L-MoS₂ at every temperature. The defect (D), trion (T) and neutral A exciton (A_{1s}) are indicated in (b). (c) Temperature dependence of PL enhancement factor (α) of A_{1s} exciton and trion peaks of 1L-MoS₂/SnSe₂ junction (J2) with 532 nm excitation, and A_{1s} exciton peak of 1L-MoS₂/TaS₂ (J4) with 633 nm excitation.

	Stack (A/B)	PL enhancement factor (α)							
		Resonant excitation (633 nm)				Non-resonant excitation [532 nm / (1040/2) nm]			
		150K		294K		150K		294K	
		$t_B \sim 8-20$ nm	$t_B \sim 20-40$ nm	$t_B \sim 8-20$ nm	$t_B \sim 20-40$ nm	$t_B \sim 8-20$ nm	$t_B \sim 20-40$ nm	$t_B \sim 8-20$ nm	$t_B \sim 20-40$ nm
Single - photon excitation	1L-MoS ₂ /SnSe ₂	0.9	---	14	0.75	0.42	---	5	0.35
	1L-WSe ₂ /SnSe ₂	---	---	---	---	0.64	---	3	0.62
	1L-WSe ₂ /SnSe ₂	---	---	0.96	---	---	---	0.5	---
	2L-MoS ₂ /SnSe ₂	---	0.23	---	0.45	---	0.17	---	0.3
	1L-MoS ₂ /hBN/SnSe ₂	---	---	4	0.182	---	---	0.54	0.154
	1L-MoS ₂ /TaS ₂	---	0.35	---	0.32	---	0.32	---	0.33
Two - photon excitation	1L-MoS ₂ /SnSe ₂	---	---	---	---	---	---	7.5	---
	1L-MoS ₂ /hBN/SnSe ₂	---	---	---	---	---	---	2.4	---

Table 1: Luminescence enhancement summary. Summary of averaged luminescence intensity enhancement factor (α) values from multiple layered heterostructures measured under varying excitation types (single versus two photons), excitation wavelength (resonant versus non-resonant), temperature, and thickness of the donor layer. The red and green shading of the boxes are for quick reference indicating quenching and enhancement, respectively. Single-photon non-resonant excitation is performed with 532 nm while two-photon non-resonant excitation is performed with 1040 nm.

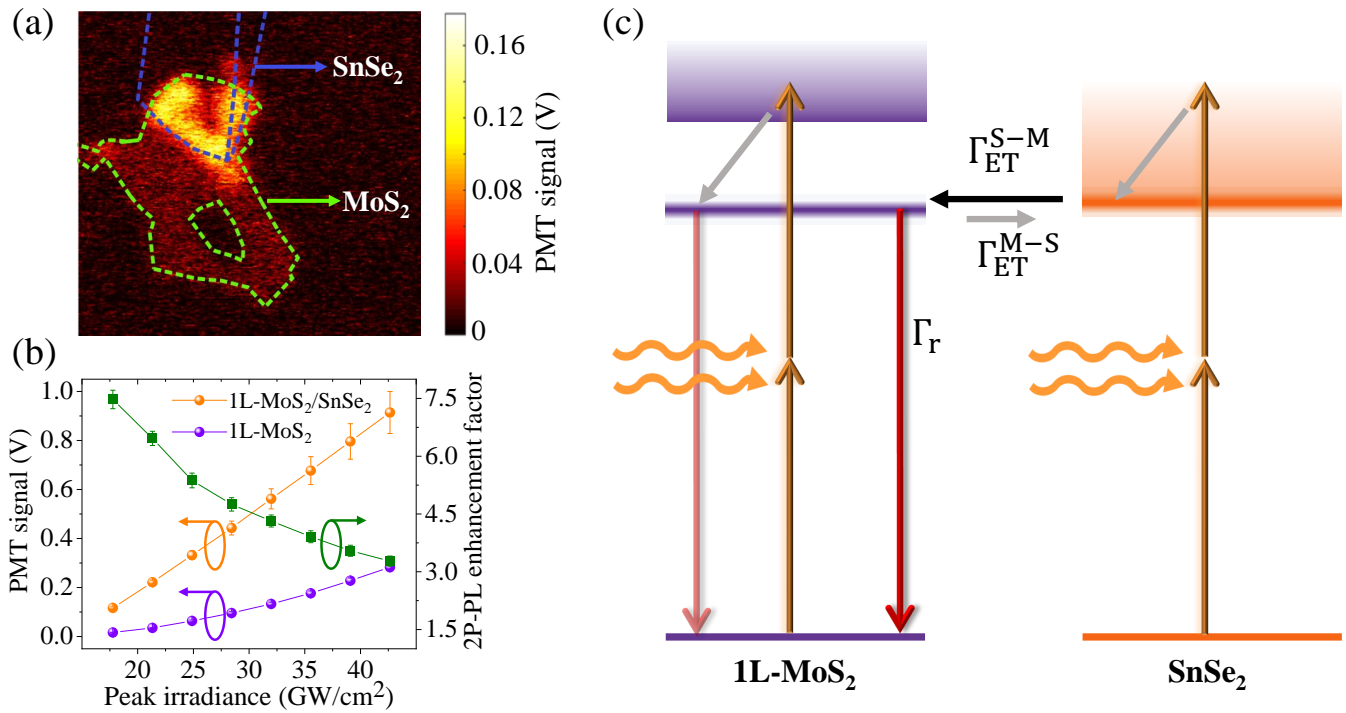


Figure 5: Two-photon luminescence enhancement. (a) Two-photon PL map of 1L-MoS₂(green) / SnSe₂(blue) of sample J1 of Fig.1(c) at 650 nm under two-photon excitation with 1040 nm laser at a peak irradiance of 17.8 GW/cm². Two-photon PL intensity corresponds to the voltage detected by Photo Multiplier Tube (PMT) whose range is represented by the color bar. (b) PMT detected voltage (left axis) of the two-photon PL of isolated 1L-MoS₂ and 1L-MoS₂/SnSe₂ junction, and the enhancement factor at the junction (right axis) as a function of peak irradiance of the excitation. (c) Transitions in 1L-MoS₂, SnSe₂ and across the junction with non-resonant two-photon excitation.

Supporting Information

Strong Single- and Two-Photon Luminescence Enhancement by Non-Radiative Energy Transfer across Layered Heterostructure

Medha Dandu, Rabindra Biswas, Sarthak Das, Sangeeth Kallatt, Suman Chatterjee,
Mehak Mahajan, Varun Raghunathan, Kausik Majumdar*

Department of Electrical Communication Engineering, Indian Institute of Science, Bangalore
560012, India

*Corresponding author, email: kausikm@iisc.ac.in

Different layered heterostructures used for PL measurements and Raman characterization

Figure S1a shows the optical image of the 1L-MoS₂/SnSe₂ junction (sample J1) used for PL spectroscopy and mapping. 1L-MoS₂ is characterized with Raman spectroscopy with 532 nm for A_{1g} and E_{2g}¹ modes which were obtained at 404.8 cm⁻¹ and 385.1 cm⁻¹ respectively.¹ Raman shift at the SnSe₂ region shows its E_g and A_{1g} peaks at 110.6 cm⁻¹ and 184.8 cm⁻¹ respectively. On the junction region, A_{1g} and E_{2g}¹ modes of 1L-MoS₂ are quenched completely as shown in Figure S1b. Figure S1c and S1d show the optical images of 1L-MoS₂/TaS₂ and 1L-Ws₂/SnSe₂ junctions used for PL characterization in this work.

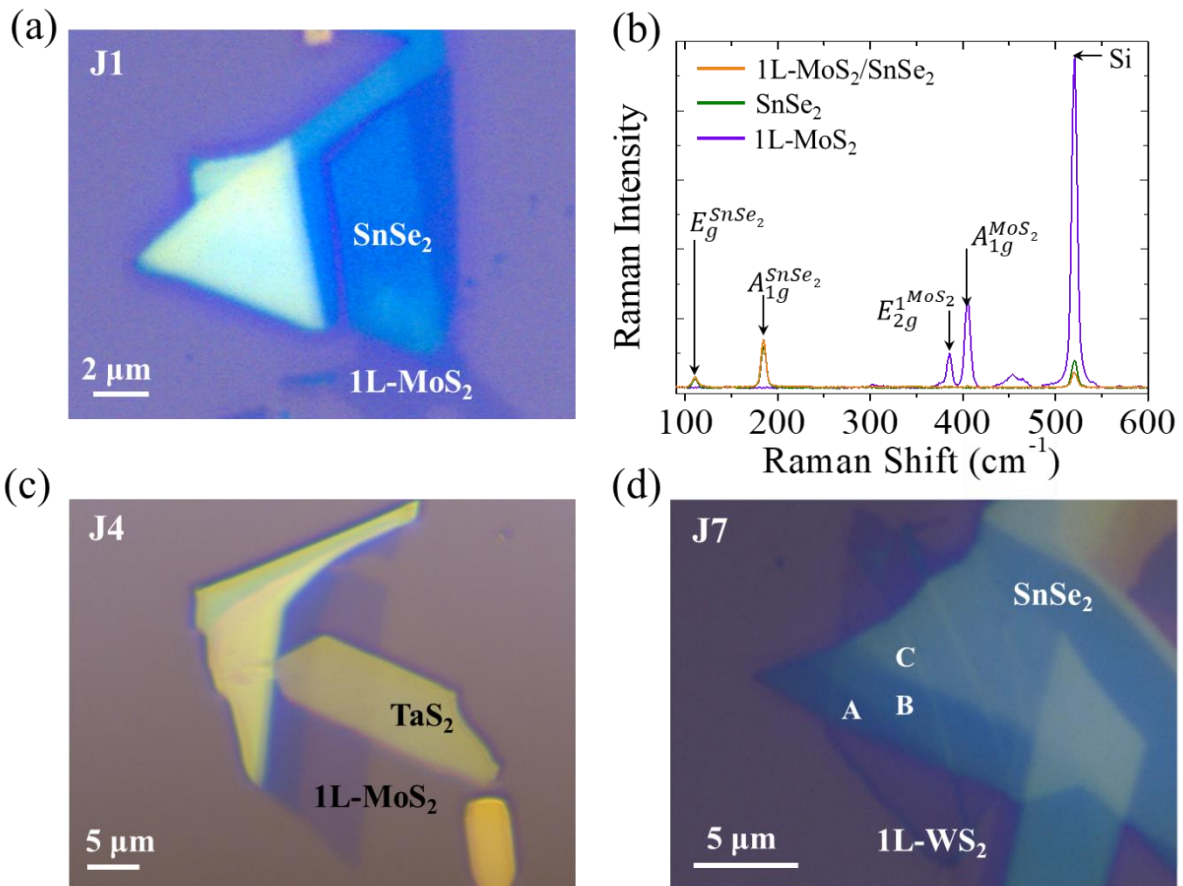


Figure S1: (a) Optical image of the 1L-MoS₂/SnSe₂ junction (J1) described in Figure 1a. (b) Raman shift of 1L-MoS₂, SnSe₂ and the junction from sample J1 characterized with 532 nm laser. (c) Optical image of the 1L-MoS₂/TaS₂ junction J4 whose spectra are represented in Figure 1f. (d) Optical image of the 1L-Ws₂/SnSe₂ junction J7 described in figure 2e-f.

PL enhancement across 1L-MoS₂/SnSe₂ from multiple samples (J2 and J3)

PL enhancement of 1L-MoS₂ on 1L-MoS₂/SnSe₂ junction is verified across other samples J2 and J3 with both 633 nm and 532 nm excitation.

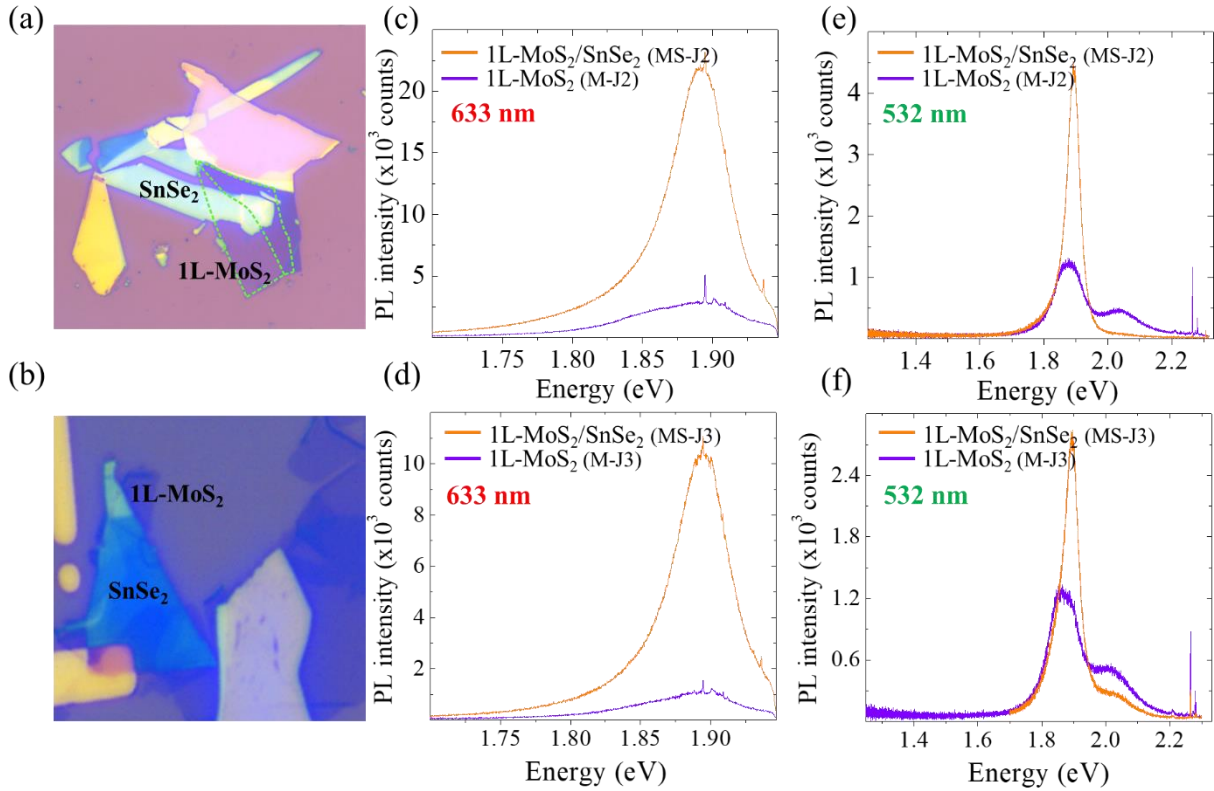


Figure S2: (a-b) The optical images of 1L-MoS₂/SnSe₂ junctions from samples J2 and J3. Sample J2 is used to characterize temperature dependence of PL enhancement. (c-d) 633 nm PL spectra of isolated 1L-MoS₂ (violet) and junction (orange) regions. (e-f) 532 nm PL spectra of isolated 1L-MoS₂ (violet) and junction (orange) regions.

Photoluminescence spectroscopy across another 1L-MoS₂/hBN/SnSe₂ sample (J6)

Due to the manifestation of efficient FRET across 1L-MoS₂/SnSe₂, PL enhancement persists even with insertion of spacer layer, hBN as discussed in the main text from sample J5. We verify this PL enhancement with both 633 nm and 532 nm across 1L-MoS₂/hBN/SnSe₂ with another sample J6.

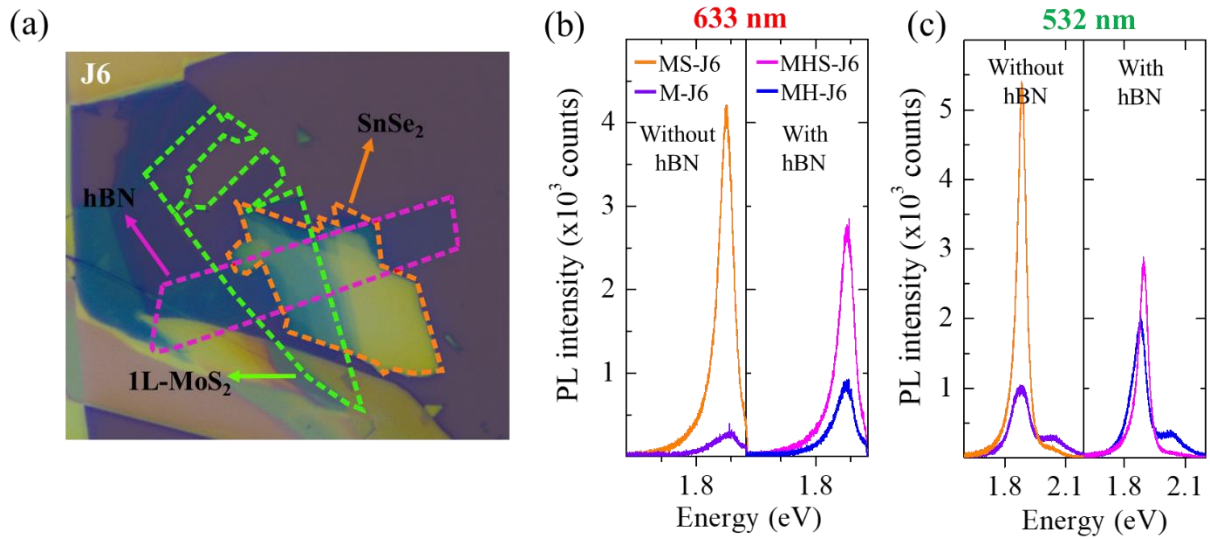


Figure S3: (a) Optical image of sample J6 used to verify PL enhancement of 1L-MoS₂ on the 1L-MoS₂/hBN/SnSe₂ junction. (b-c) 633 nm and 532 nm PL spectra of 1L-MoS₂/SnSe₂ junction and the corresponding isolated 1L-MoS₂ control without (left panel) and with the presence of hBN (right panel) in the sample J6.

Reflectance contrast of SnSe₂ at low temperature

Reflectance contrast spectra of SnSe₂ flakes of different thickness on SiO₂/Si substrate are also measured at 4K. The dip in the reflectance contrast is found to change its spectral position with SnSe₂ thickness as observed at room temperature. Even at this low temperature, the dip is still spectrally broad and does not show any sharp excitonic feature. This helps to confirm that transition dipole in SnSe₂ is governed by free electron-hole pairs as the screening offered by the large carrier concentration suppresses strongly bound exciton state in SnSe₂.

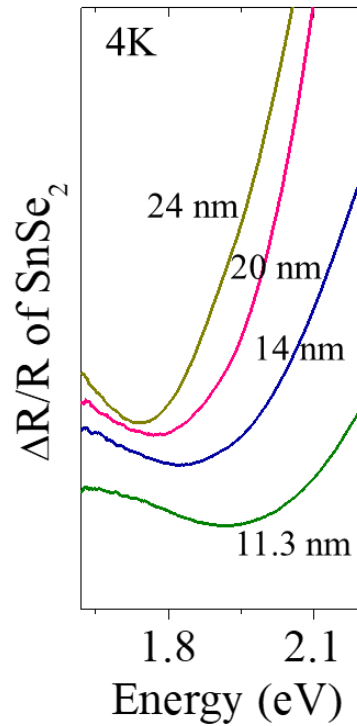


Figure S4: Reflectance contrast spectra of isolated SnSe₂ flakes on SiO₂/Si substrate at 4 K. Corresponding thickness of SnSe₂ is indicated at each spectrum.

Photoluminescence spectroscopy across 2L-MoS₂/SnSe₂

Unlike 1L-MoS₂, 2L-MoS₂ does not exhibit any PL enhancement on the junction with SnSe₂. Figure S5a shows the quenched PL spectra of 2L-MoS₂/SnSe₂ with 633 nm at different temperatures. From Figure S5b we can see that there is decrease in PL quenching with increase in temperature like that of 1L-MoS₂/SnSe₂. The absence of PL enhancement in the case of 2L-MoS₂/SnSe₂ can be correlated with the competition between the rate of FRET and increased non-radiative scattering in bilayer as seen from the model in the next section.

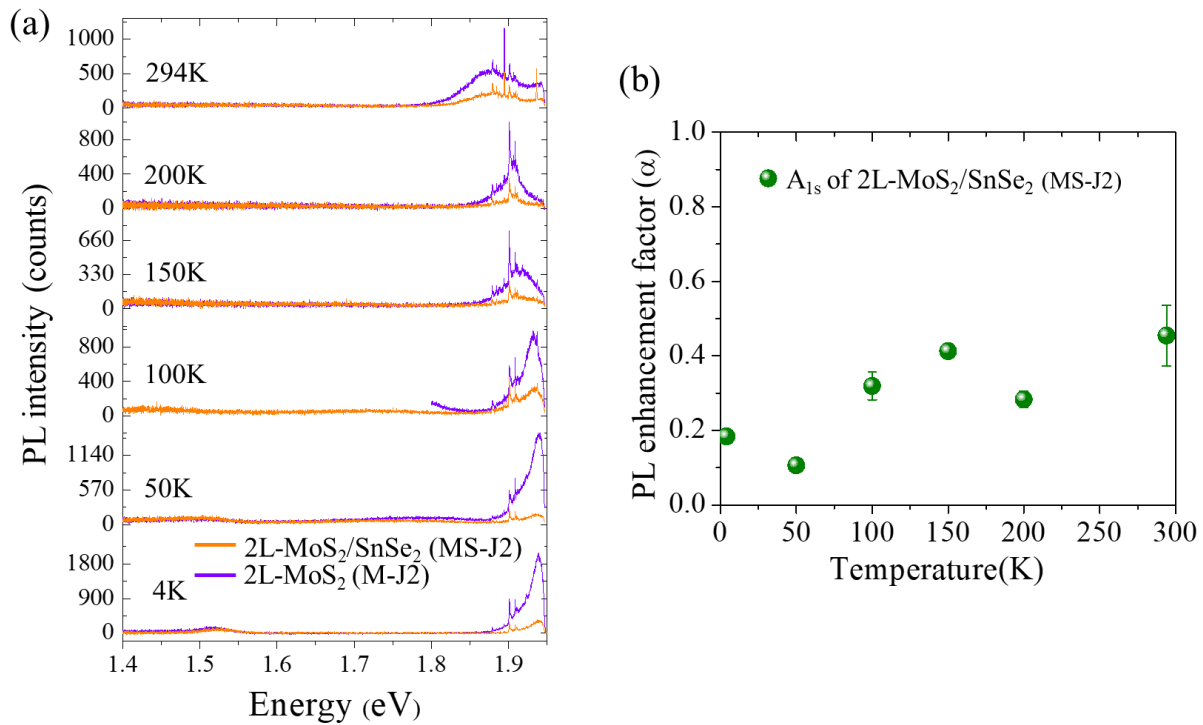


Figure S5: (a) Temperature dependent PL spectra of 2L-MoS₂ (violet) and its junction with SnSe₂ (orange) from sample J2 under 633 nm excitation. (b) Variation of PL enhancement factor (α) of A_{1s} exciton peak of 2L-MoS₂/SnSe₂ with 633 nm excitation.

Discussion on the rate of FRET and PL enhancement factor

Deriving PL enhancement factor from the rate equations:

Experimental data proves that the PL enhancement observed across different layered heterostructures is sensitive to excitation wavelength (resonant versus non-resonant), temperature, donor and acceptor materials, thickness of the donor and the acceptor, and the separation between them. To get a qualitative understanding of the effect of these parameters, we derive an expression for the PL enhancement factor from the rate equations of exciton density in the isolated 1L-MoS₂ and the 1L-MoS₂/SnSe₂ junction.

Rate equations for Monolayer MoS₂ on SiO₂ with resonant excitation:

633 nm excitation near resonantly excites the exciton states of 1L-MoS₂. Let G_{ex}^{M} be the generation rate of A_{1s} excitons with 633 nm in 1L-MoS₂ on SiO₂. These excitons can either recombine radiatively at a rate Γ_{r} to give out photoluminescence or decay non-radiatively at a rate $\Gamma_{\text{nr}}^{\text{M}}$. The non-radiative decay (Γ_{nr}) comprises of scattering to the defect states at lower energies and scattering to the energy states outside the light cone as schematically shown in Figure 4b. The rate equation for the exciton density (N_{ex}^{M}) density in isolated 1L-MoS₂ on SiO₂ can be written as the following.

$$\frac{dN_{\text{ex}}^{\text{M}}}{dt} = G_{\text{ex}}^{\text{M}} - (\Gamma_{\text{r}} + \Gamma_{\text{nr}}^{\text{M}})N_{\text{ex}}^{\text{M}} \quad (1)$$

The steady state photoluminescence signal from a given excitation will be proportional to the fraction of steady state exciton density, $N_{\text{ex}}^{\text{M}} = \frac{G_{\text{ex}}^{\text{M}}}{(\Gamma_{\text{r}} + \Gamma_{\text{nr}}^{\text{M}})}$ decaying radiatively. So, the PL intensity from 1L-MoS₂ on SiO₂ is given to be

$$I_{\text{M}} \propto \frac{G_{\text{ex}}^{\text{M}} \Gamma_{\text{r}}}{(\Gamma_{\text{r}} + \Gamma_{\text{nr}}^{\text{M}})} \quad (2)$$

Rate equations for Monolayer MoS₂ on SnSe₂ with resonant excitation:

As shown in the schematic, 633 nm near resonantly excites multi-layer SnSe₂ along with 1L-MoS₂. This excitation creates free electron hole pairs in SnSe₂ at its direct bandgap at a rate $G_{\text{e-h}}^{\text{S}}$ (not excitons because of screening of carriers in the degenerately doped SnSe₂). These free electron

hole pairs are coupled to the A_{1s} exciton states via FRET at a rate of Γ_{ET}^{S-M} or they can be scattered from the energy states in SnSe₂ (resonant to A_{1s} of MoS₂) to other non-resonant energy states predominantly to the states at the indirect band gap at a rate Γ_s . Excitons in 1L-MoS₂ either excited with 633 nm on the junction or created with FRET from SnSe₂ will also be coupled to the states in SnSe₂ through the process of FRET and thus they can decay to SnSe₂ by this dipole-dipole coupling at a rate denoted by Γ_{ET}^{M-S} . Electrons and holes from exciton state in MoS₂ can also dissociate to lower energy states in conduction and valence bands of SnSe₂ which causes decay of excitons through charge transfer at a rate of Γ_{CT}^{M-S} . The non-radiative decay rate of excitons on the junction Γ_{nr}^{jun} can be different from Γ_{nr}^M as seen from the change of broadening of PL peaks on the junction. However, the radiative decay rate Γ_r is assumed to be similar in 1L-MoS₂ and the junction. Generation rate of free e-h pairs in SnSe₂ and excitons in MoS₂ on the junction are assumed to be similar to the rates in individual layers. From the above discussion, the rate equations for exciton density in 1L-MoS₂ on the junction ($N_{ex}^{M,jun}$) and free e-h pair density in SnSe₂ ($N_{e-h}^{S,jun}$) can be expressed as

$$\frac{dN_{ex}^{M,jun}}{dt} = G_{ex}^M - (\Gamma_r + \Gamma_{nr}^{M,jun} + \Gamma_{CT}^{M-S} + \Gamma_{ET}^{M-S})N_{ex}^{M,jun} + \Gamma_{ET}^{S-M}N_{e-h}^{S,jun} \quad (3)$$

$$\frac{dN_{e-h}^{S,jun}}{dt} = G_{e-h}^S - (\Gamma_s + \Gamma_{ET}^{S-M})N_{e-h}^{S,jun} + (\Gamma_{CT}^{M-S} + \Gamma_{ET}^{M-S})N_{ex}^{M,jun} \quad (4)$$

Since an order of enhancement is seen in the PL intensity of 1L-MoS₂ on the junction, the contribution of G_{ex}^M in (3) can be neglected. From (3) and (4), $I_{M,jun}$ can be obtained from $N_{ex}^{M,jun}$ as

$$N_{ex}^{M,jun} = \frac{G_{e-h}^S \Gamma_{ET}^{S-M}}{\Gamma_s (\Gamma_r + \Gamma_{nr}^{M,jun} + \Gamma_{CT}^{M-S} + \Gamma_{ET}^{M-S}) + \Gamma_{ET}^{S-M} (\Gamma_r + \Gamma_{nr}^{M,jun})} \quad (5)$$

$$I_{M,jun} \propto N_{ex}^{M,jun} \Gamma_r \quad (6)$$

The PL enhancement factor, α is the ratio of steady state PL intensity of A_{1s} peak from 1L-MoS₂/SnSe₂ ($I_{M,jun}$) to that of 1L-MoS₂ on SiO₂ (I_M).

$$\alpha = \frac{\left(\frac{G_{e-h}^S}{G_{ex}^M}\right) \Gamma_{ET}^{S-M}}{\Gamma_s \left(\frac{\Gamma_r + \Gamma_{nr}^{M,jun}}{\Gamma_r + \Gamma_{nr}^M} + \frac{\Gamma_{CT}^{M-S} + \Gamma_{ET}^{M-S}}{\Gamma_r + \Gamma_{nr}^M} \right) + \Gamma_{ET}^{S-M} \left(\frac{\Gamma_r + \Gamma_{nr}^{M,jun}}{\Gamma_r + \Gamma_{nr}^M} \right)} \quad (7)$$

To get a preliminary insight into the role of different rate parameters on α , it is reasonable to ignore the difference between $\Gamma_{nr}^{M,jun}$ and Γ_{nr}^M . α can now be expressed as

$$\alpha = \left(\frac{G_{e-h}^S}{G_{ex}^M}\right) \frac{\gamma}{\gamma + \beta} \quad (8)$$

where $\gamma = \frac{\Gamma_{ET}^{S-M}}{\Gamma_s}$ and $\beta = 1 + \left(\frac{\Gamma_{CT}^{M-S} + \Gamma_{ET}^{M-S}}{\Gamma_r + \Gamma_{nr}^M}\right)$.

Temperature dependence of the rate of FRET:

As seen from eq-(7), variation of α with temperature can be related to the temperature dependent rate of different processes on illumination. Γ_{CT} and Γ_r are very weakly dependent on the temperature while Γ_{ET} and Γ_{nr} that vary with temperature can play a role in determining the value of α . We adopt the energy transfer model by Lyo² based on dipole-dipole coupling across quantum wells to understand the temperature dependence of α in our case. This model deals with the energy transfer from an exciton to a free e-h pair which predicts its rate as

$$\Gamma_{ET} = \Gamma_{ET}^0(\xi_T) g\left(\frac{d}{\xi_T}\right) \quad (9)$$

where d is the physical separation between the donor and the acceptor layers and ξ_T is a temperature dependent parameter, $\xi_T = \sqrt{\frac{\hbar^2}{2Mk_B T}}$ where k_B is the Boltzmann constant and M is the total mass of exciton ($M=m_e+m_h$) which is assumed to be same for both the layers.

$\Gamma_{ET}^0(\xi_T) = \frac{32\pi\mu}{\hbar^3} \left(\frac{q^2 D_1 D_2}{\kappa a_B \xi_T}\right)^2$ which depends the system of donor and acceptor with μ as reduced exciton mass, a_B is the exciton bohr radius, κ is the average dielectric constant, D_1 and D_2 are the dipole moments of the donor and the acceptor. $g(t)$ is expressed as

$$g(t) = \int_0^{\infty} x^3 e^{-x^2} e^{-2tx} S(tx)^2 dx \quad (10)$$

with $s(t) = \frac{\sin(\frac{tb_1}{2d})}{\frac{tb_1}{2d}} \frac{\sin(\frac{tb_2}{2d})}{\frac{tb_2}{2d}}$, where b_1 and b_2 are the thickness of the donor and the acceptor respectively. To project the variation of FRET in our case, we assume that rate of energy transfer is of similar magnitude in both the directions across MoS₂ and SnSe₂ and therefore (9) can be applicable to calculate both Γ_{ET}^{S-M} and Γ_{ET}^{M-S} . Assuming $b_1=10$ nm (SnSe₂), $b_2=1$ nm (MoS₂), $d=1$ nm and $M \sim m_0$ in SnSe₂,³ we obtain the temperature dependence of Γ_{ET} as shown in Figure S6a. Using the above variation of Γ_{ET} and (8) with assumption of parameters $\Gamma_{CT} = 10^{12} \text{ s}^{-1}$, $\Gamma_{nr} + \Gamma_r = 0.5 \times 10^{12} \text{ s}^{-1}$, $\Gamma_s = 10^{13} \text{ s}^{-1}$ and $\left(\frac{G_{e-h}^S}{G_{ex}^M}\right)=10$, an evaluation of α is done at multiple temperature which matches with the trend of experimental data as in Figure S6b.

(8) also explains the absence of enhancement for trion in 1L-MoS₂ from the interplay between FRET and radiative recombination. As Figure S6c shows the variation of α with Γ_{ET} and Γ_r keeping all other rate parameters fixed. $\alpha > 1$ for those cases where $\beta < \gamma$ which indicates that Γ_r should be fast enough to yield luminescence of FRET coupled dipoles in the acceptor. It has been shown experimentally that trion has a longer life time than exciton which makes Γ_r of exciton higher than that of trion.⁴ This increased lifetime of trion accelerates their loss from MoS₂ to SnSe₂ and hinders the luminescence of trions from energy transferred dipoles.

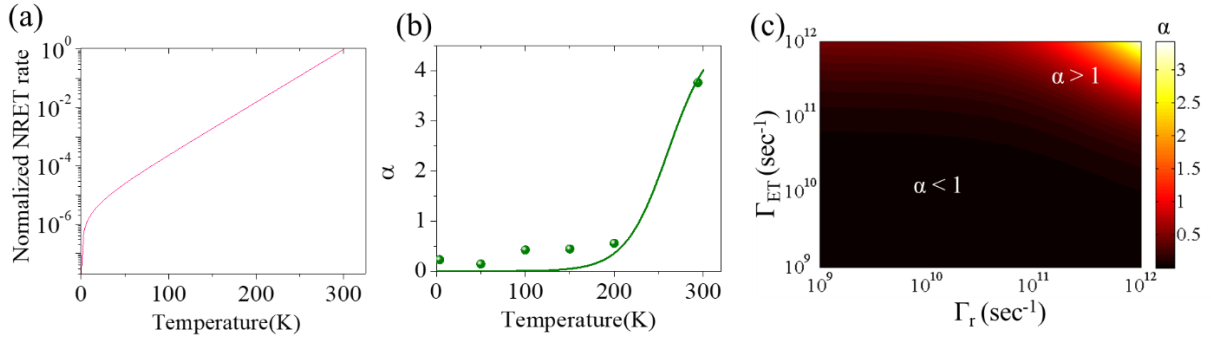


Figure S6: (a) Variation of the rate of FRET with temperature calculated from theoretical model. The y-axis is normalized with respect to the FRET rate at 300K. (b) Experimental (symbol) and model predicted (line) values of enhancement factor (α) calculated at different temperatures with 532 nm excitation. (c) Color plot of variation of enhancement factor (α) with change in the rate of FRET and the rate of radiative recombination. The enhancement ($\alpha > 1$) and quenching ($\alpha < 1$) regions are indicated.

References:

- (1) Chakraborty, B.; Matte, H. S. S. R.; Sood, A. K.; Rao, C. N. R. Layer-Dependent Resonant Raman Scattering of a Few Layer MoS₂. *J. Raman Spectrosc.* **2013**, *44*, 92–96.
- (2) Lyo, S. K. Energy Transfer of Excitons between Quantum Wells Separated by a Wide Barrier. *Phys. Rev. B - Condens. Matter Mater. Phys.* **2000**, *62*, 13641–13656.
- (3) Gonzalez, J. M.; Oleynik, I. I. Layer-Dependent Properties of SnS₂ and SnSe₂ Two-Dimensional Materials. *Phys. Rev. B* **2016**, *94*, 125443.
- (4) Wang, H.; Zhang, C.; Chan, W.; Manolatu, C.; Tiwari, S.; Rana, F. Radiative Lifetimes of Excitons and Trions in Monolayers of the Metal Dichalcogenide MoS₂. *Phys. Rev. B* **2016**, *93*, 045407.